Supporting information:

SUPER-RESOLUTION FINGERPRINTING DETECTS CHEMICAL REACTIONS AND IDIOSYNCRASIES OF SINGLE DNA PEGBOARDS

Alexander Johnson-Buck[1], Jeanette Nangreave[2,3], Do-Nyun Kim[4], Mark Bathe[4], Hao Yan[2,3] and Nils G. Walter[1]*

[1]Department of Chemistry, 930 N. University Ave., University of Michigan, Ann Arbor, MI 48109-1055, USA.

[2]The Biodesign Institute, Arizona State University, Tempe, Arizona 85287, USA

[3]Department of Chemistry and Biochemistry, Arizona State University, Tempe, Arizona 85287, USA

[4]Department of Biological Engineering, MIT, Cambridge, MA 02139

*nwalter@umich.edu

Table of Contents

Materials and Methods

Unless otherwise noted, all chemicals were purchased from Fisher and all oligonucleotides were purchased from Integrated DNA Technologies (IDT). Analysis of PAINT experiments, including plotting and reconstruction, was performed using home-written MATLAB code unless stated otherwise.

Preparation of DNA origami scaffolds. Rectangular DNA origami arrays consist of an M13mp18 viral DNA scaffold (New England Biolabs) and 202 ssDNA staples as previously described[1]. For all structures assembled here, staples 1-12 and 205-216 were omitted to prevent inter-array base stacking interactions that result in undesirable aggregation (Figure S1). Of the remaining staples, several were modified at their 5′-end with an additional sequence, 5′-ACC TCT CAC CCA CCA TTC ATC, to which the substrate **S** (5′-GAT GAA TGG TGG GTG AGA GGT TTT TCA CTA TrAG GAA GAG) can bind (Table S1). The arrays were annealed in either 2x HBS buffer (300 mM NaCl, 20 mM HEPES, pH 7.4) or 5x SSC (750 mM NaCl, 75 mM Trisodium Citrate, pH 7.4) buffer, with a 1:3 ratio of M13 to staple strands and a final concentration of 10 nM (M13). There is no apparent difference in the assembly of arrays using these two buffer conditions. The arrays were annealed over 12 hours from 94°C-25°C using a PCR thermocycler (Eppendorf). The template origami **R** or **L** was incubated with a 3:1 ratio of substrate **S** to available binding sites on the origami prior to AFM imaging. Integrity of the ribose moiety of **S** was verified by subjecting this oligonucleotide to denaturing PAGE in 8 M urea alongside an equivalent sample that had been incubated for 15 minutes in sodium phosphate buffer, pH 12, at 75°C and subsequently staining with SYBR Gold (Invitrogen) per the manufacturer's instructions (Figure S12).

Atomic force microscopy characterization of DNA origami scaffolds and assembled pegboards. 2 μL of annealed sample was deposited on a freshly cleaved mica surface (Ted Pella, Inc.) and left to adsorb for two minutes. After adsorption, 400 μL of buffer (1x TAE-Mg^{2+}: 40mM Tris, 20 mM acetic acid, 12.5mM Mg2+, pH 7.6) was added to the liquid cell and the sample was scanned in peak-force mode, using ScanAsyst in liquid probes, on a Veeco Multimode 8 AFM. All imaging by AFM was carried out at room temperature. The resulting AFM images were processed/flattened and analyzed with NanoScope Analysis software (Veeco, version 1.40). To determine the yield of DNA origami scaffold formation, ~1μM x ~1μM AFM images were evaluated. Each DNA origami structure in the AFM images was assigned to one of the following three categories, based on the height features present in the images: 1) well-formed tile with clear evidence of fairly complete track, 2) well-formed tile with defective or missing track, or 3) broken or deformed tile. Only those DNA origami tiles with clearly discernible boundaries were considered (i.e. not cut-off like those at the edges of the AFM images, not obscured by impurities in the sample, and not stacked/clustered together). Estimated yields for **R** and **L** origami are shown in Table S2.

Preparation of PAINT probes and other fluorescently labeled DNA. Oligonucleotides were ordered with terminal amine modifications for fluorescent labeling: probe **α-NH_2**, 5′-/5aminoC6/ATA GTG AAA; probe **β-NH_2**, 5′-/5aminoC6/CTC

TTC CTA; **S-NH_2**, 5′-GAT GAA TGG TGG GTG AGA GGT TTT TCA CTA TrAG GAA GAG /3AmMO/. **S-NH_2** was ordered HPLC purified, and all three oligonucleotides were used as provided without further purification. The oligonucleotides were labeled with *N*-hydroxysuccinimidyl ester derivatives of Cy3 or Cy5 (GE Healthcare) by overnight incubation in $NaHCO_3$, pH 8.3, followed by ethanol precipitation and thorough washing with 80% ethanol until the supernatant was colorless. Denaturing polyacrylamide gel electrophoresis revealed no detectable free dye. Labeling efficiency was quantified by absorbance at 280 nm and either 550 nm (Cy3) or 650 nm (Cy5) using a Beckman DU 640B Spectrophotometer, and exceeded 85% for all strands except for **β-Cy3**, for which it was 30%. Labeling efficiency less than unity does not hamper PAINT experiments due to the continuous exchange of unlabeled probes for labeled ones. Cy3-labeled 8-17 DNAzyme (**8-17-Cy3**), 5′-/5Cy3/TCT CTT CTC CGA GCC GGT CGA AAT AGT GAA AA, was ordered with HPLC purification and used as-is for binding kinetics assays.

Preparation of microscope slide surface for fluorescence microscopy and PAINT. Quartz microscope slides (3” x 1” x 1 mm, G. Finkenbeiner) were prepared as described[2]. Briefly, ~1 mm holes were drilled approximately 3 cm apart to create inlet and outlet ports for a flow channel. The slides were cleaned by sonicating in 1 M KOH, followed by heating in a solution of 5% hydrogen peroxide (Acros, 202460010) and 5% ammonium hydroxide (Acros, 205840025). The slides were rinsed thoroughly with deionized water and flamed for approximately 1 min using a propane torch. To prepare the surface for conjugation to NeutrAvidin, the slides were silanized by incubating for 1 hour in a 5% (v/v) solution of (3-aminopropyl)triethoxysilane (Sigma-Aldrich, A3648) in acetone, rinsed thoroughly with acetone, and cured at 80°C for 1 hour. The bisfunctional cross-linking agent para-diisothiocyanate (PDITC, Acros, 417510050) was then conjugated to the free amines of the aminosilane by immersing the slides in a 0.2 % (w/v) solution of PDITC in a 1:10 mixture of pyridine:*N,N*-dimethylformamide for 2 hours. The slides were washed thoroughly with methanol (Acros, 610090040) followed by acetone. Finally, to conjugate NeutrAvidin by its surface amines to the PDITC, a 0.5 mg/mL solution of NeutrAvidin (Invitrogen, A-2666) in 50 mM NaCl, 1 mM EDTA, 10 mM Tris-HCl, pH 8.0 was applied to each slide and incubated in a humid environment for 2 hours. The slides were washed with a solution of 1 M NaCl and 40 mM NaOH for 1 minute to quench free isothiocyanate, rinsed thoroughly with deionized water, and dried under nitrogen. A fluidic channel between the two drilled holes was formed over the NeutrAvidin-coated portion of each slide using double-sided tape (Scotch, permanent 1/2") and coverslips (VWR, 24 x 30 mm, No. 1.5), then sealed with 5-minute Epoxy (Hardman Adhesives, 4001). The slides were stored in a desiccated chamber at 4 °C for up to 4 weeks. Prior to an experiment, inlet and outlet ports were constructed on a slide using sterile 200 µL pipet tips inserted into the drilled holes (Eppendorf) and ~ 5-cm lengths of microbore tubing (Cole-Parmer, EW06418-05), and sealed with Epoxy.

Total internal reflection fluorescence microscope. Assembly kinetics and all PAINT experiments were carried out on an inverted total internal reflection (TIRF) fluorescence microscope with a 1.2 NA 60x water-immersion objective (IX71, Olympus) in an environmentally controlled room at 20 ± 3 °C. Cy3 excitation was provided by a 532-nm

green laser (ultra-compact diode-pumped Nd:YAG laser GCL-025-S, CrystaLaser, 5 W/cm^2 for kinetic measurements and 60 W/cm^2 for PAINT measurements) and Cy5 excitation by a 638-nm red diode laser (Coherent CUBE 635-25C, 4 W/cm^2 for kinetic measurements, and Olympus LAS/640/100-D, 100 W/cm^2 for PAINT measurements). Excitation was continuous in all experiments. The Cy3 and Cy5 emission signals were separated by a dichroic mirror with a cutoff wavelength of 610 nm (Chroma) and projected side-by-side onto an ICCD camera chip (iPentamax HQ Gen III, Roper Scientific, Inc.). Relay lenses matched the microscope image with the camera focal plane and the IX71 internal 1.6x magnifier (final effective pixel length 133 nm). The Cy3 channel image was passed through a band pass filter (HQ580/60m, Chroma) and the Cy5 channel was passed through a long pass filter (HQ655LP, Chroma). A Newport ST-UT2 vibration isolation table was used in all experiments.

Characterization of kinetics of origami pegboard assembly and S cleavage by 8-17 DNAzyme. A 10 nM solution of **R** template origami in 5x HEPES-buffered saline (HBS; 1x HBS ≡ 150 mM NaCl, 10 mM HEPES-KOH, pH 7.0-7.4) was diluted to 100 pM in 1x HBS, flowed into the channel of a NeutrAvidin-coated slide, and allowed to bind via the biotin-NeutrAvidin interaction for 10 min. The excess origami was washed out twice with 1x HBS. While monitoring the fluorescence of Cy3 at the slide surface using the TIRF microscope, a solution of 100 nM **S-Cy3** in 1x HBS containing oxygen scavenger system[3] (OSS ≡ 2.5 mM 3,4-dihydroxybenzoic acid, Sigma P5630; 1 mM Trolox, Acros 218940050; and 25 nM protocatechuate dioxygenase, Sigma-Aldrich P8279) was injected into the slide channel with a dead time of less than 10 s. To limit photobleaching, the excitation light was passed through a neutral density filter (OD 2.0, Newport Model 5215) and a shuttered illumination scheme was used with 0.5-s exposures separated by 14.5-s dark periods. The **S-Cy3** was injected during a dark period. The mean fluorescence signal from 382 origami was plotted as a function of time (Figure S3a) and fit to the single-exponential model $y = C(1 - e^{k'_{obs}t})$.

To measure the cleavage of **S-Cy3** by 8-17 DNAzyme (**8-17**) at the ensemble level, a 1x HBS solution containing 1 μM **8-17** (5′- CTC TTC TCC GAG CCG GTC GAA ATA GTG AAA A, used as-is from IDT), 1 mM $ZnSO_4$, and OSS was added to the slide already containing **R** origami saturated with **S-Cy3** while observing *via* the same shuttered illumination scheme described above. Upon the addition, the Cy3 fluorescence signal from each origami began to attenuate. The signal was averaged across all origami and plotted as a function of time. The decay was not well modeled by a single-exponential decay function, but was well fit to the double-exponential model $y = C_1\left(e^{k'_{obs,1}t}\right) + C_2\left(e^{k'_{obs,2}t}\right)$ (Figure S3b). The signal decrease due to photobleaching is minimal under these illumination conditions, as is evidenced by the nearly horizontal signal intensity prior to **8-17** addition at time *t*=0. The decline in signal is not significantly different from the time course measured by PAINT under the same cleavage conditions (Figure 3c).

In order to perform the time-course measurements of **S** cleavage using PAINT, it was necessary to remove the **8-17** DNAzyme after each interval of cleavage to make **S** available for binding by **α** and **β**. To determine the kinetics of **8-17** dissociation from **S**-

loaded **R** origami, a mixture of 5 nM **R** template origami and 3.8 μM **S** was incubated in 250 mM NaCl, 25 mM HEPES-KOH, pH 7.4 at room temperature for 10 minutes. The origami were then diluted to 100 pM in 1x HBS, flowed into the channel of a NeutrAvidin-coated slide, and allowed to bind for 10 minutes. Excess sample was flushed away by two washes with 1x HBS. Then, a solution containing 1x HBS , 100 nM **8-17-Cy3**, and OSS was added to the slide channel until apparent saturation was achieved, as judging by the increase in Cy3 fluorescence intensity of each origami (20 minutes). Finally, the dissociation kinetics of **8-17** were measured by monitoring the decrease in Cy3 fluorescence upon addition of 1x HBS containing OSS and 1 μM unlabeled **S** to compete with origami-bound **S** for **8-17-Cy3** under shuttered, attenuated illumination as described above. The intensity of Cy3 from many origami was averaged and modeled well by a single-exponential model (Figure S3c). According to the resulting rate constant, approximately 80% of bound **8-17** is expected to dissociate from full-length **S** over the course of 1 hour.

Characterization of PAINT probe binding kinetics on DNA origami pegboards. A mixture of 5 nM template origami and 3.8 μM **S** (a 6:1 ratio between **S** and binding sites for **S** on the origami) was incubated in 250 mM NaCl, 25 mM HEPES-KOH, pH 7.4 at room temperature for 10 minutes. The origami was then diluted to 100 pM in 1x HBS, flowed into the channel of a NeutrAvidin-coated slide, and allowed to bind via the biotin-NeutrAvidin interaction for 10 minutes. Excess sample was flushed away by two washes with 1x HBS.

The slide was mounted on the TIRF microscope, and a solution containing OSS, 1x HBS, and 1 or 2.5 nM each of **α-Cy3** and **β-Cy5** was added to the slide channel. After a 2-minute incubation to permit equilibration of [O_2], the binding of the PAINT probes was visualized under excitation at 532 nm and 640 nm with a camera exposure time of 1 s. To limit photobleaching, excitation power was reduced to ~10% of the power used in PAINT experiments. Doubling the excitation power did not yield significantly different first-order rate constants.

Intensity time traces for Cy3 and Cy5 were analyzed using the hidden Markov modeling software package vbFRET[4] to extract idealized trajectories. A single exponential decay function, $y = Ce^{kt}$, was fit to the histograms of dwell times in the bound and unbound states to yield the dissociation rate constant k_{off} and pseudo-first-order association rate constant k_{on}', respectively. The values of k_{on}' were plotted as a function of concentration, fit to linear increase functions, yielding the second-order association constant k_{on} as the slope. The results from duplicate trials are shown in Table S2.

PAINT nanoscopy of DNA origami pegboards. R or **L** origami template was loaded with **S** and immobilized on a NeutrAvidin-coated slide as in the characterization of PAINT probe kinetics, above. The slide was mounted on the TIRF microscope, and a solution containing OSS, 1x HBS, and 10-20 nM of **α-Cy3** and/or **β-Cy5** (or **α-Cy5** and **β-Cy3**) was added to the slide channel. After a 2-minute incubation to allow equilibration of [O_2], the binding of the PAINT probes was visualized under excitation at 532 nm and 640 nm with a camera exposure time of 1 s. Imaging proceeded for 1000-4000 s.

Generation of PAINT reconstructions. Individual origami tiles were located in the field of view by the repeated appearance of Cy3 and/or Cy5 signal in the same location. Specifically, a fluctuation map (Figure S4) was generated by subtracting each movie frame from the preceeding frame, taking the absolute value of the intensity differences, and averaging across all movie frames to obtain the average frame-to-frame fluctuation in intensity at each pixel. This allowed us to distinguish origami, as sites of repeated PAINT probe binding, from other bright fluorescent contaminants. The origami appeared as bright diffraction-limited spots in this fluctuation map, and were localized by Gaussian fitting to obtain coordinates of all origami in a field of view.

For each origami, traces of intensity as a function of time (Figure 1e) were generated as follows. In each movie frame, a 5x5-pixel square region ***A*** centered on each origami was defined. The background fluorescence, determined from the median of the 24 pixels immediately surrounding ***A***, was subtracted from each pixel within ***A***. The background-corrected intensity values within ***A*** were summed to obtain the total fluorescence intensity of probe(s) bound to an origami tile in a given movie frame. During the generation of intensity traces, the region ***A*** was re-defined if the microscope stage drifted by more than one pixel, or 133 nm, in the x or y direction (see below).

The microscope stage drifted by 50-250 nm in the x-y plane throughout a typical experiment (Figure S5). To correct for this, each movie was divided into 100- to 200-s bins and the intensity of all the frames within each bin was averaged. The time-averaged image from each bin was cross-correlated with time-averaged image from the first bin in the movie with 100-fold up-sampling using the MATLAB script dftregistration[5]. Linear interpolation yielded an estimate of the microscope stage drift in each movie frame (Figure S5b).

During movie frames in which a DNA origami's fluorescence intensity exceeded a threshold (500-2000 photons/s, depending on the experiment and excitation intensity), the intensity profile was fit to a 2-dimensional Gaussian function of the form

$$I = Ce^{-\frac{(x-\mu_x)^2}{2\sigma_x{}^2}-\frac{(y-\mu_y)^2}{2\sigma_y{}^2}} + b \qquad \text{(S1)}$$

to extract the centroid (μ_x,μ_y), as well as parameters for localization error estimation, including point-spread function widths σ_x and σ_y and a more precise photon count ($2\pi C\sigma_x\sigma_y$). A 7x7-pixel fitting box centered on the origami was used for fitting. Gaussian fits were filtered for quality and were rejected if any of the following criteria were met:

1. Either σ_x and σ_y exceeded a cutoff of 2 pixels (266 nm).
2. The residual between the fit and the actual intensity profile within the fitting box exceeded 25% of the total volume of the Gaussian fit.

This helped to reduce the influence of aberrant fits resulting from nonspecific binding of probes to the slide surface in the vicinity of the origami. Fitting error was estimated as described[6], using the parameters derived from each fit as well as the standard deviation

of the background signal and the effective pixel size of 133 nm. Multiple fits from the same binding event were combined by taking the median of all centroid measurements ($\mu_{x,i},\mu_{y,i}$) for that event to avoid multiple counting of a single binding event.

To generate PAINT reconstructions, the set of all position measurements (μ_x,μ_y) for an origami was enumerated. The microscope stage drift was subtracted from each position measurement. Then, a reconstruction was generated as a sum of Gaussian functions on a grid of 4-nm square pixels, with the centroid of each Gaussian representing a drift-corrected position measurement. The width parameters σ_x and σ_y for the reconstruction Gaussians were defined as the median error for all position measurements for a given origami.

When characterizing dense fields of targets, the quality of the reconstructions is often limited by sampling density rather than localization error. Therefore, on the basis of Poisson statistics, we found it convenient to define a sampling radius σ_{sample} and used it as a lower bound for the reconstruction Gaussian widths σ_x and σ_y:

$$\sigma_{sample} = \sqrt{\frac{\lambda}{\pi\rho}} = \sqrt{\frac{\lambda A}{N\pi}} \qquad \text{(S2)}$$

Where λ is the desired number of localizations per sampling area of $\pi\sigma^2$, and $\rho=N/A$ is the actual sampling density consisting of N localizations over the object area A. With λ = 2, 85% of the available binding sites will lie within σ_{sample} of a localization, assuming equal sampling probability of all binding sites. Using λ = 2, we calculated σ_{sample} for each origami and used it as a lower bound for the error values used in the reconstruction. For instance, if 100 localizations are counted for an object approximately 60 x 100 nm in size, $\sigma_{sample} = \sqrt{\frac{12000}{100\pi}}$ = 6 nm, which is comparable to the theoretical localization error in our experiments. In other words, resolution was limited by sampling unless N exceeded ~100. Consistent with this observation, simulated PAINT images of origami show rapid improvement in reconstruction quality, as quantified by deviation from an idealized reconstruction, as N increases from 10 to 200, with marginal improvements thereafter (Figure S6).

For two-color PAINT reconstructions, the binding distributions of α and β binding had to be registered in the same coordinate space due to the fact that they were detected *via* different sets of optics projecting the image onto separate regions of the CCD camera. First, a coarse third-order polynomial mapping was found between the two channels using Gaussian fitting of fiduciary markers with fluorescence visible in both channels (FluoSpheres 580/605, Invitrogen, F-8810). The registration error[7], calculated as the average distance between the calculated and actual positions of the Cy5 centroid based on the polynomial mapping from Cy3 coordinates, was 10-20 nm. An initial two-color overlay of the PAINT reconstructions was generated using this mapping. To further fine-tune the registration, the PAINT reconstructions from Cy3 and Cy5 were registered directly by cross-correlation[5] (Figure S9a-d). To reduce the influence of uneven binding

(heterogeneous binding or sampling noise) on registration, the reconstruction in each channel was saturated at 10% of its maximal intensity value for purposes of registration. For all experiments except for those involving cleavage of substrate by a DNA enzyme, the Cy3 and Cy5 reconstructions were normalized such that their total integrated intensity was equal to unity for final visualization.

Identification of origami pegboard patterns from PAINT reconstructions. Samples consisting of **R** or **L** origami were synthesized and their identities concealed. Each sample was imaged in the presence of 10 nM **β-Cy5** for 1000 s, and reconstructions generated from the resulting 20-60 localizations per origami as described above. Origami reconstructions were visually inspected and classified as linear, rectangular, or other as follows:

1. Linear: between 50 and 150 nm in length, less than 50 nm wide, only one main segment of intensity visible.
2. Rectangular: between 50 and 150 nm in size in both dimensions, at least three sides of a rectangle visible.
3. Other: neither of the above two criteria satisfied.

The results of this classification are shown in Figure 2e.

PAINT time course of S cleavage by 8-17 DNAzyme on individual R origami. R origami were assembled with **S** and deposited on NeutrAvidin slides as described above. The origami were first imaged in the presence of 1x HBS containing OSS and 10 nM each of **α-Cy3** and **β-Cy5** for 33 minutes. Then, a solution of 1x HBS containing 1 μM **8-17** and 1 mM $ZnSO_4$ was added to the slide channel and incubated for 2 minutes. The slide channel was flushed with 1x HBS containing 1 μM unlabeled **S** to stop the reaction and sequester any remaining **8-17** in solution. After 60 minutes, the sample was imaged again in the presence of **α-Cy3** and **β-Cy5** for 33 minutes. A solution of 1 μM **8-17** and 1 mM $ZnSO_4$ was once again added to the slide channel and incubated for 8 minutes. The slide channel was flushed with 1 μM unlabeled **S** again and incubated for 60 minutes. Finally, the sample was imaged for the third time in the presence of **α-Cy3** and **β-Cy5**. Two-color PAINT images of origami were reconstructed and analyzed as described above (Figure 3b). The total number of binding events for **α-Cy3** and **β-Cy5** (N_α and N_β, respectively) were compared at different time points to quantify the fraction of **S** that had been cleaved after each incubation with **8-17** and Zn^{2+} (Figure 3c).

Model-free 2D alignment of R origami reconstructions. To characterize the population-level heterogeneity of PAINT reconstructions of **R** origami, the refine2d functionality of EMAN v1.9 was used. Reconstructions from **β-Cy5** binding to 198 **R** origami pooled from three independent experiments were cropped to equal-size square images and subjected to 10 iterations of model-free alignment assuming between 2 and 10 classes. All runs converged before the 10^{th} iteration. Inspection of the output revealed that fewer than 9 classes resulted in some smearing or loss of features (e.g., disappearance of the empty region in the center of the **R** rectangle), while more than 8 classes produced more nearly degenerate classes. Although the results from using 9

classes (Figure S7) show some possible degenerate class averages (e.g. panels g and h), this was the lowest number of classes that recapitulated the diversity of reconstructions observed. Approximately 45% of the origami (panels a, c, d, and f) fall into classes that approximate an open rectangular shape, which is similar to the percentage of apparently rectangular shapes observed in the **R** vs. **L** comparison (Figure 2) and the yield estimates by AFM (Table S3). Although limited contrast hinders characterization of **S** pattern completeness by AFM, several AFM images of **R** origami show patterns that resemble the class averages (lower right corner of each panel in Figure S7), suggesting that at least some of the heterogeneity across origami is due to incomplete assembly of the origami scaffold or pegboard. This is consistent with the fact that the distribution of total binding events per origami within a single experiment is broader than would be expected for identical, perfectly assembled origami (Figure S8).

Characterization of spatial homogeneity of PAINT probe binding to individual R origami. When a rectangular **S** pattern is divided into four quadrants containing equal areas of **S**, if binding is homogeneous, the number of probe binding events observed in each quadrant follows a Poisson distribution with a single expectation value across all quadrants. The homogeneity of binding across the four quadrants can thus be characterized using

$$\chi^2 = \sum_{i=1}^{4} \frac{(I_i - \bar{N})^2}{\bar{N}} \quad \text{(S2)}$$

Where I_i is the observed number of binding events in quadrant *i* and $\bar{N}$ is the expected number of binding events per quadrant, estimated as the average across all four quadrants. Assuming a Poisson-distributed probability of binding to each quadrant, χ^2 can be approximated by a chi-squared distribution with 3 degrees of freedom[8].

To automatically divide each origami into equal quadrants, the two registered reconstructions from Cy3 and Cy5 probe binding were summed to yield a combined reconstruction R_{comb}. Again, to reduce the influence of uneven binding, R_{comb} was saturated at 10%. The reconstruction R_{comb} was aligned to the cardinal axes by finding its edges *via* the Sobel method in the MATLAB Image Processing Toolbox and rotating the edge map in 1-degree increments to find the angle of maximal cross-correlation to a 60-by-100-nm rectangular mask (Figure S9e-f). The angles of rotation for all origami in a given movie are uniformly distributed, as expected for origami deposited in random orientations (Figure S2). The aligned R_{comb} was then divided into four quadrants so as to minimize χ^2. Finally, the same rotation and division were applied to the raw Cy3 and Cy5 reconstructions, the number of localizations falling into each quadrant counted, and χ^2 calculated for each channel (Figure S9g-h).

Verifying sequence dependence of binding heterogeneity. R origami were imaged with the probe set (**α-Cy3** + **β-Cy5**) for about 66 min. The same origami were then imaged in the presence of the inversely labeled probe set (**β-Cy3** + **α-Cy5**) for about 66 minutes. Hence, there is an approximately 1 h delay between the reconstructions generated from the two probe sets. Reconstructions from Cy3- and Cy5-labeled probes

were generated and registered as described above, and the reconstruction from each channel was normalized to a total intensity of unity. No angular rotation was performed. The reconstruction from Cy5 was then subtracted from the Cy3 reconstruction to yield a difference map (Figure S10). The two difference maps were aligned by cross-correlating the combined reconstructions R_{comb} for the two probe sets, and the 2-D correlation coefficient $R(\Delta I_{\alpha\beta}, \Delta I_{\beta\alpha})$ between the difference maps was calculated.

Simulation of PAINT reconstructions. Numerical simulations to predict the properties of PAINT reconstructions as a function of imaging parameters, and to interpret experimental results, were conducted as follows. Virtual PAINT probes were allowed to bind at random with uniform probability to virtual binding sites with spatial patterns defined by the designs shown in Figure 1. Each PAINT probe was "localized" by perturbing the coordinates of the binding site with random Gaussian-distributed variables with standard deviations defined by the localization error (6-10 nm, reflective of typical experimental values). A reconstruction was generated according to the procedure used for experimental PAINT measurements as described above (Figure S6a,b). In cases of two-color simulations, two independent reconstructions were generated for each origami. For Figure 4d-e, the simulated origami arrays were randomly oriented and the reconstructions subjected to the same automated alignment, registration, and analysis procedures as the experimental reconstructions. In simulations of 1000 **R** origami with 100 binding events per tile, the alignment error was ± 3.3° (s. d.).

Prediction of three-dimensional solution shape of DNA origami pegboard. The three-dimensional equilibrium solution shape of R origami was predicted using the finite element-based model CanDo (**C**omputer-**a**ided e**n**gineering for **D**NA **o**rigami, http://cando-dna-origami.org) using default geometric parameters for B-form DNA (0.34 nm axial rise per basepair, 2.25 nm diameter helix, 10.5 basepair per turn helicity) and mechanical properties (stretching, bending, and torsional stiffnesses of 1100 pN, 230 pN nm^2, and 460 pN nm^2, respectively)[9,10]. We modeled immobilization of the biotin anchor sites of the pegboard to the microscope slide via biotin-NeutrAvidin complexes by fixing pegboard displacements at the biotin anchor sites (i.e., to keep the biotinylated positions mutually coplanar). As a control to compare the effect of fixing these displacements we also analyzed the pegboard without any biotin anchor site constraints (Figure S15).

Modeling of local substrate concentration on R origami. 17-base substrate oligonucleotides were modeled as freely-jointed chains with end-to-end vector described by the standard Gaussian probability density function

$$P(\vec{r}) = \left(\frac{3}{2\pi\langle\vec{r}^2\rangle}\right)^{3/2} e^{-\frac{3\vec{r}^2}{2\langle\vec{r}^2\rangle}}$$

where $\vec{r}$ is the end-to-end vector of the ssDNA segment and $\sqrt{\langle \vec{r}^2 \rangle} = \sqrt{N_k} l_k = L l_k$ is the root-mean-square end-to-end distance with the number of Kuhn segments (N_k), the Kuhn length (l_k), and contour length (L). Effects of three-dimensional solution shapes of R origami on local substrate concentrations were characterized by calculating the volume of overlap between adjacent spheres centered at the tip of 20-base-pair DNA duplex whose radius was chosen to be the root-mean-square end-to-end distance of 17-base single-stranded region of the substrate ($\sqrt{\langle \vec{r}^2 \rangle}$ = 3.6 nm, Figure S16)[11]. The double-stranded portion of the substrate was modeled as a rigid rod normal to the pegboard surface as its contour length (~7 nm) is much less than the persistence length of dsDNA (~50 nm). The normalized volume overlap at each substrate location was calculated using

$$V_{n,i} = \frac{\sum_{j \neq i} V_{o,ij}}{V_{ref}}$$

where $V_{n,i}$ denotes the normalized volume overlap at substrate i, $V_{o,ij}$ represents the volume of overlap between spheres at substrates i and j, and V_{ref} is the reference volume set to be $\frac{4}{3}\pi\sqrt{\langle \vec{r}^2 \rangle}^3 = 195$ nm^3.

Figure S1: Rectangular Origami Tile for Pegboard Construction

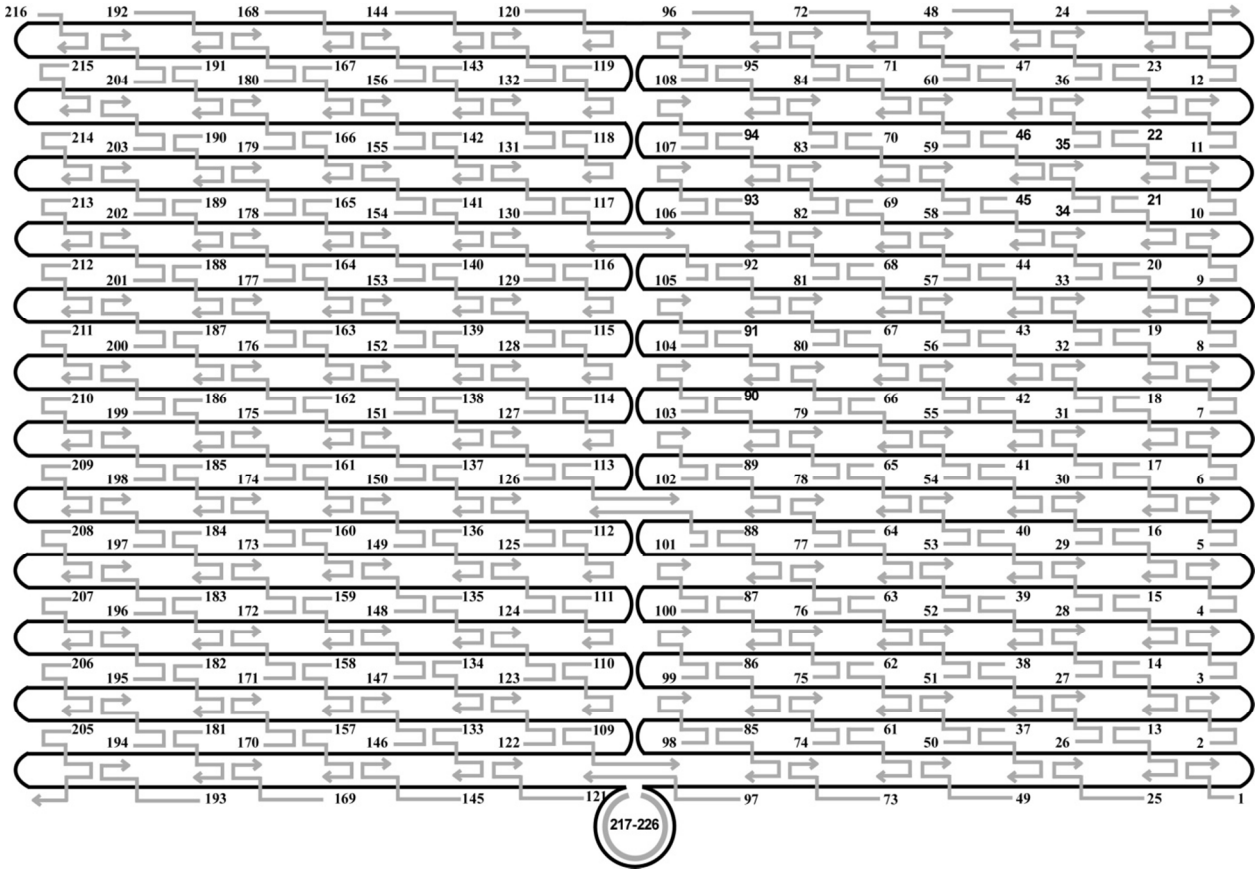

Schematic representation of a rectangular origami tile. The continuous black line represents the circular M13 viral genome and the gray lines correspond to unmodified staples with arrows pointing toward the 3′ ends. Each staple is labeled with a number at the 5′ end that corresponds to the sequences listed in Table S1.

Figure S2: Angles of Rotation for 117 R Origami in One Movie

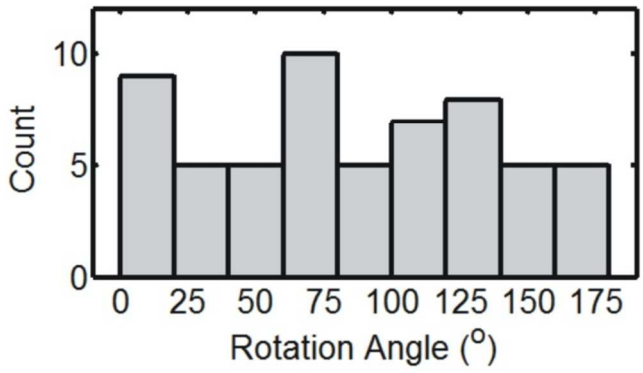

Unidirectional rotation angle providing optimal alignment with a 60 x 100 nm rectangular mask for 117 **R** origami. The distribution is isotropic ($\chi^2(8, N = 117) = 4.9$, $P = 0.76$), consistent with random deposition of origami on the slide surface.

Figure S3: Kinetics of Substrate Assembly, Substrate Cleavage, and Dissociation of 8-17 DNAzyme from Substrate on R Origami Pegboards

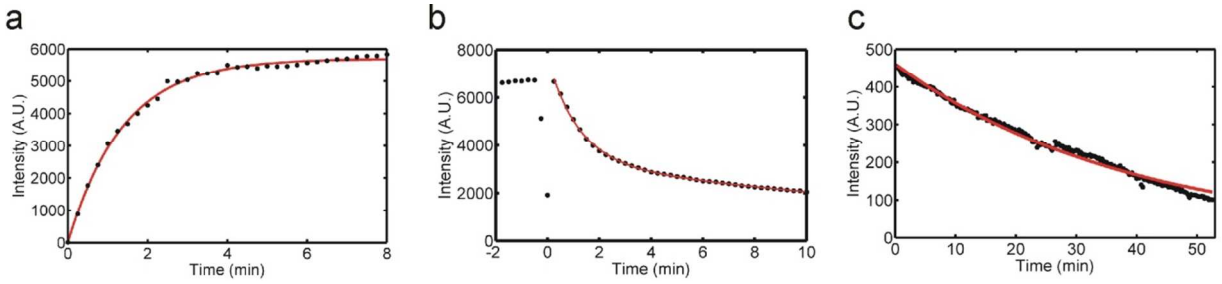

a, Fluorescence time course of 100 nM Cy3-labeled substrate (**S-Cy3**) binding to surface-immobilized **R** origami (black dots). This is a ~40-fold lower concentration of substrate and ~100-fold lower concentration of origami than that used in preparing samples for PAINT imaging. Fitting to the single exponential model $y = C(1-e^{-kt})$ yields an apparent pseudo-first-order rate constant k'_{obs} = 0.72 min^{-1} (red curve, R^2 = 0.998). The y-coordinate is the mean Cy3 fluorescence intensity of 382 origami. **S-Cy3** was added at time *t* = 0 with a dead time of < 10 s. **b,** Fluorescence time course of cleavage of **S-Cy3** on **R** origami in the presence of 1 μM 8-17 DNAzyme and 1 mM $ZnSO_4$. Fitting to a double exponential model $y = C_1(e^{-k1*t}) + C_2(e^{-k2*t})$ to the interval from 0.25-10 min (red curve, R^2 > 0.999) yields apparent rate constants of 0.83 min^{-1} (relative amplitude 0.56) and 0.05 min^{-1} (relative amplitude 0.44). The y-axis is the mean Cy3 fluorescence intensity from 259 origami. **S-Cy3** was added at time *t* = 0 with a dead time of < 10 s. The temporary drop in intensity around time *t* = 0 was caused by the sample going out of focus due to mechanical perturbations immediately prior to the addition. **c**, Fluorescence time course of dissociation of Cy3-labeled **8-17** DNAzyme from unlabeled **S** immobilized on **R** origami. Fitting to the single-exponential model $y = C(1-e^{-kt})$ yields an apparent first-order rate constant of 0.025 min^{-1} (red line, R^2 = 0.994). The y-axis is the mean Cy3 fluorescence intensity from 181 origami.

Figure S4: Fluctuation Map of a Representative Field of View Containing Origami

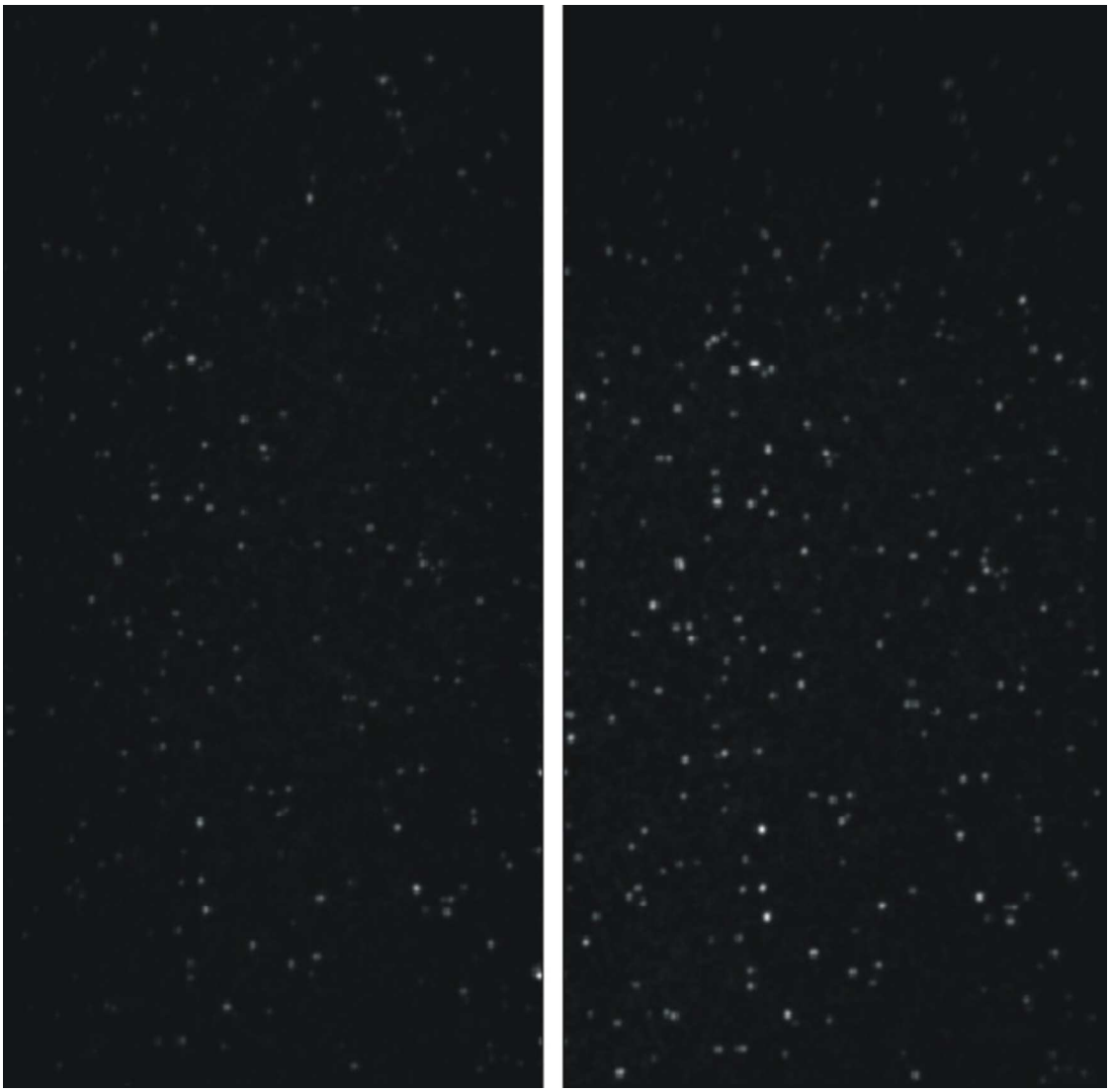

Fluctuation map for of a representative 34 x 68 μM field of view for **α-Cy3** (left half) and **β-Cy5** (right half). The intensity of each pixel in the fluctuation map is proportional to the average frame-to-frame intensity fluctuation of that pixel in the raw movie. Origami are thus localized as the sites of repeated appearance and disappearance of Cy3 and Cy5 signal, which appear as bright spots in the fluctuation map.

Figure S5: Impact of Stage Drift Correction on Reconstruction Quality

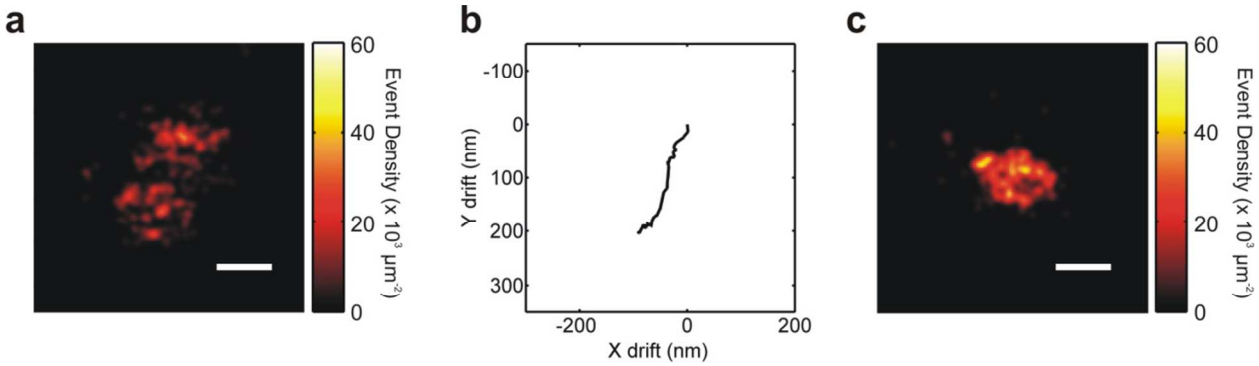

a, Monochromatic PAINT reconstruction of one **R** origami without accounting for X-Y drift of the microscope stage. **b**, Drift of the microscope stage as determined by cross-correlation between consecutive ~200-s bins of the original movie. **c,** Final reconstruction obtained by subtracting the drift (**b**) from the raw coordinates in (**a**). Scale bars in **a** and **c** are 100 nm.

Figure S6: Impact of Sampling on Reconstruction Quality

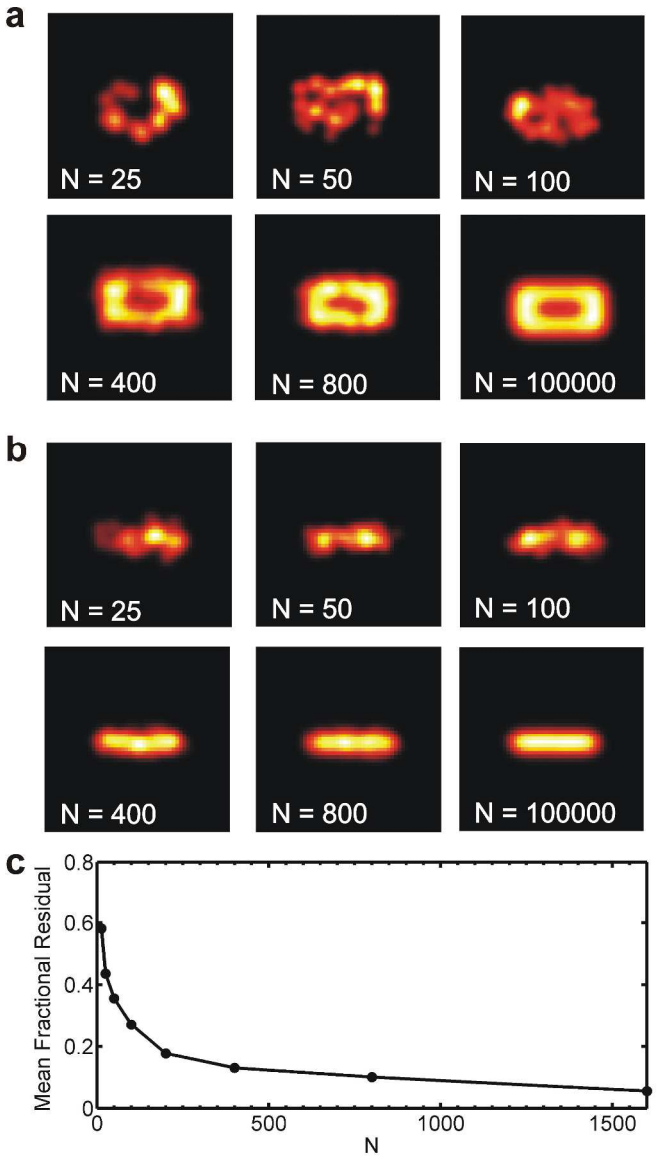

a,**b**, Representative simulated reconstructions of (**a**) **R** origami and (**b**) **L** origami with varying numbers of PAINT binding events. **c**, Mean fractional residual of **R** origami reconstructions as a function of the number of localizations, N. Residuals were calculated by subtracting the intensity profile of each reconstruction from that of an ideal reconstruction (N = 100,000, panel **a**), with all reconstructions normalized to a maximal value of 1. The residuals are expressed as a fraction of the total intensity of the ideal reconstruction. Residuals were nearly identical for **L** reconstructions (not shown).

Figure S7: Class Averages from Model-Free 2-D Refinement of R Origami Reconstructions

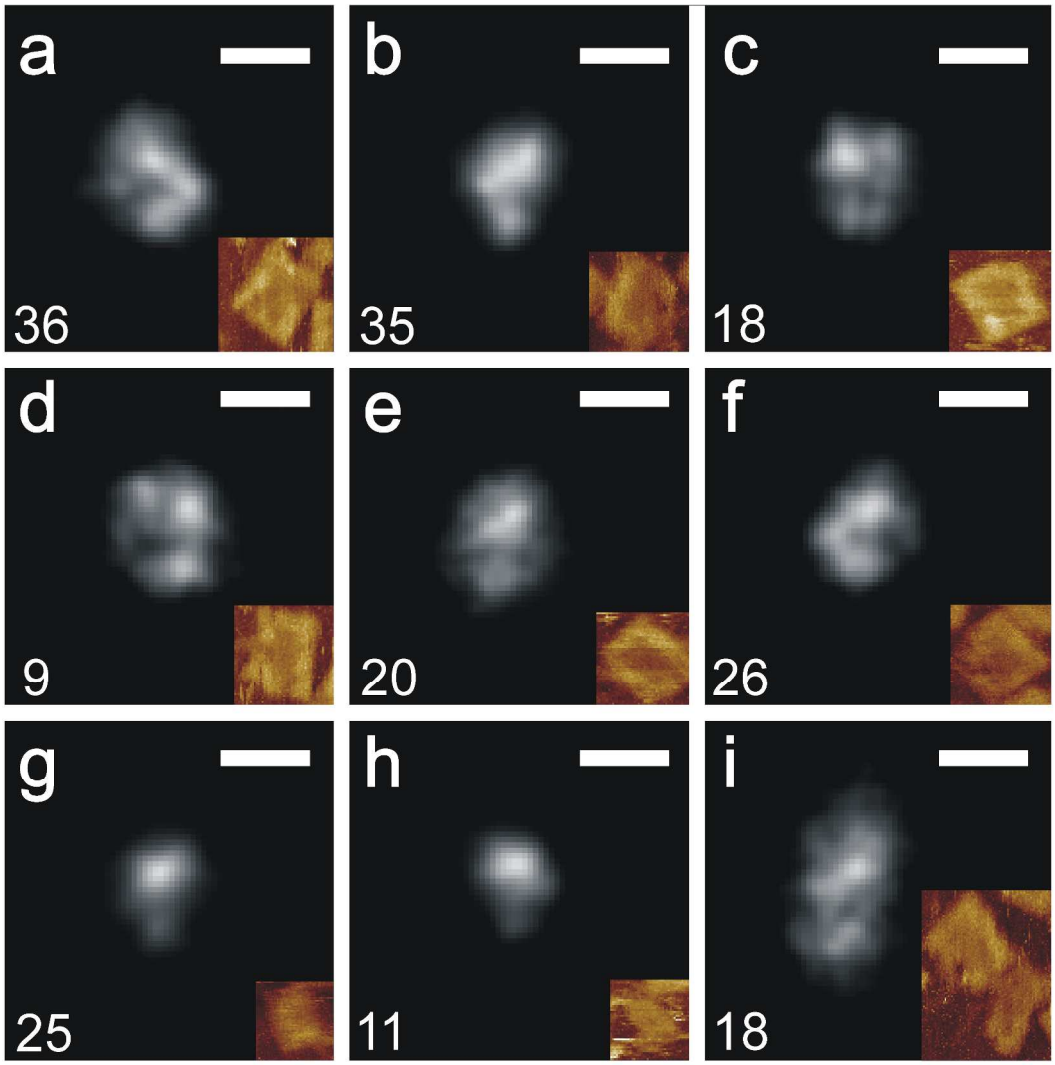

a-i, Nine class averages demonstrating the observed morphological variety in reconstructions of 198 **R** origami from **β-Cy5** binding. The number of reconstructions in a given class is indicated at the bottom center of the panel. Classes **a, c, d, f, and** possibly **e** represent well-formed origami immobilized with a relatively flat geometry parallel to the plane of the microscope slide. Scale bars (upper right of each frame): 100 nm. AFM images of **R** individual origami bearing **S** patterns comparable to each PAINT class average are shown in the lower right corner of each panel, at the same scale as the corresponding PAINT image. The class averages in panels **g** and **h** may represent origami fragments and/or incomplete immobilization (e.g., freely rotating due to being attached by only one biotin). Class average **i** may correspond to various side-by-side aggregates of origami.

Figure S8: Number of β-Cy5 Binding Events Per Origami Versus Spatial Heterogeneity of Binding

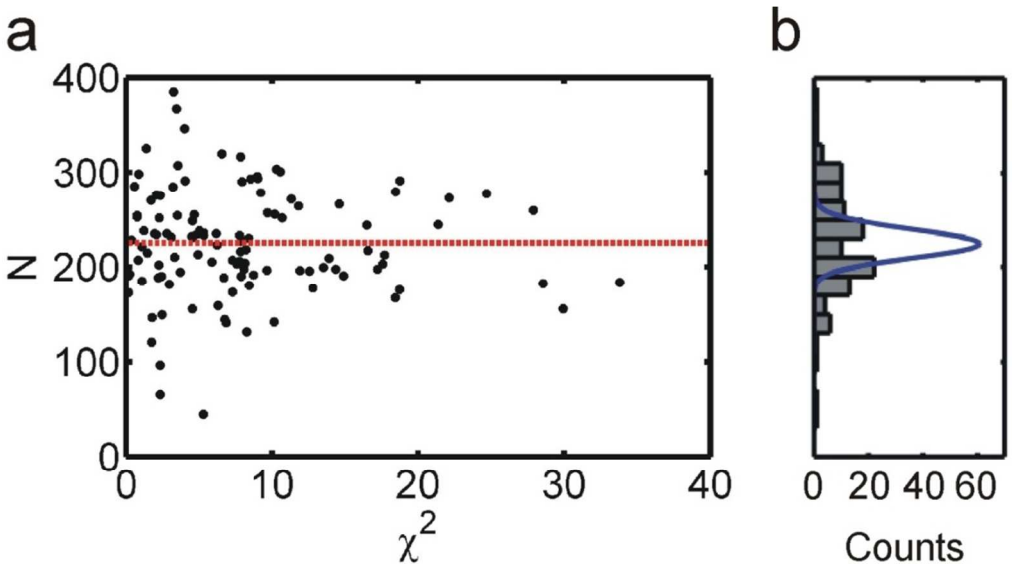

a, Chi-squared value vs. number of **β-Cy5** binding events (N) per origami for 114 **R** origami in one movie. The Pearson correlation coefficient between χ^2 and N is -0.03, demonstrating that there is no correlation between overall probe binding efficiency and measured heterogeneity. The red dashed line is the mean binding events per origami, 225 +/- 57 (s.d.). **b,** Histogram of the values of N shown in panel **a** (gray bars) as compared to the predicted Poisson distribution for identical origami. The observed distribution is significantly broader than the theoretical distribution ($\chi^2(113) = 1625$, $p < 10^{-10}$), suggesting considerable differences in the number or availability of assembled **S** strands across different origami tiles.

Figure S9: Registration and Alignment of Two-Color PAINT Reconstructions of R Origami

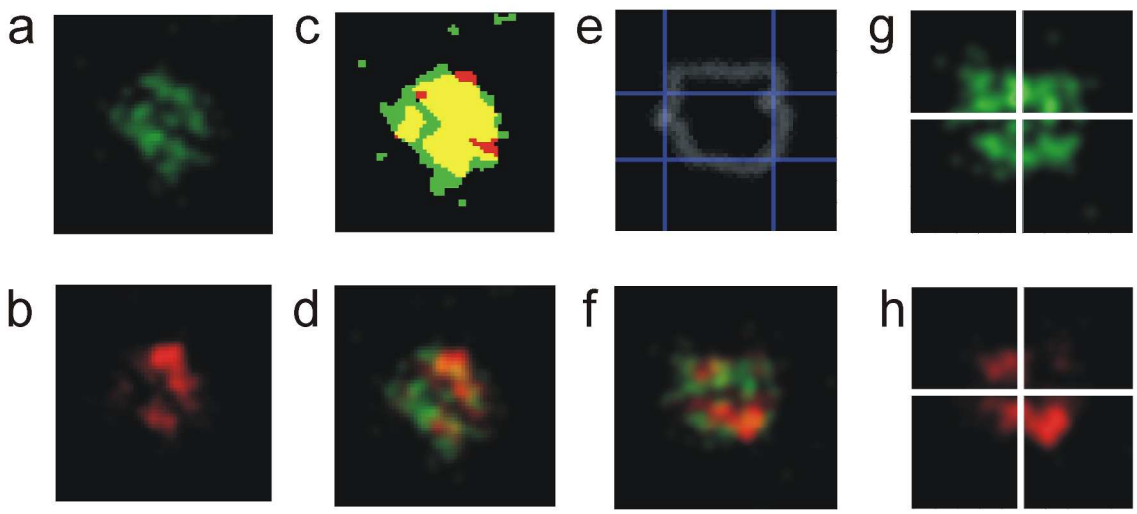

a, **b**, **c**, **d**, Drift-corrected reconstructions from Cy3 (**a**) and Cy5 (**b**) binding to a single **R** origami tile are registered by passing each through a binary filter with a threshold of 20% maximal intensity, then finding the maximal cross-correlation between the filtered images (**c**), resulting in a two-color overlay (**d**). **e**, **f**, An edge map of the origami (**e**, gray) is aligned with a 60 x 100 nm rectangular mask (**e**, blue) to align the reconstruction with the cardinal axes (**f**). The reconstruction is then divided into four quadrants, with the boundaries chosen so as to divide the area of the origami as equally as possible between the four quadrants. **g**, **h**, Finally, the divisions are applied to each channel separately to calculate χ^2 for the binding distribution of each probe.

Figure S10: Calculation of Difference Maps and Correlation Coefficients from the Binding of Inversely Labeled Probes

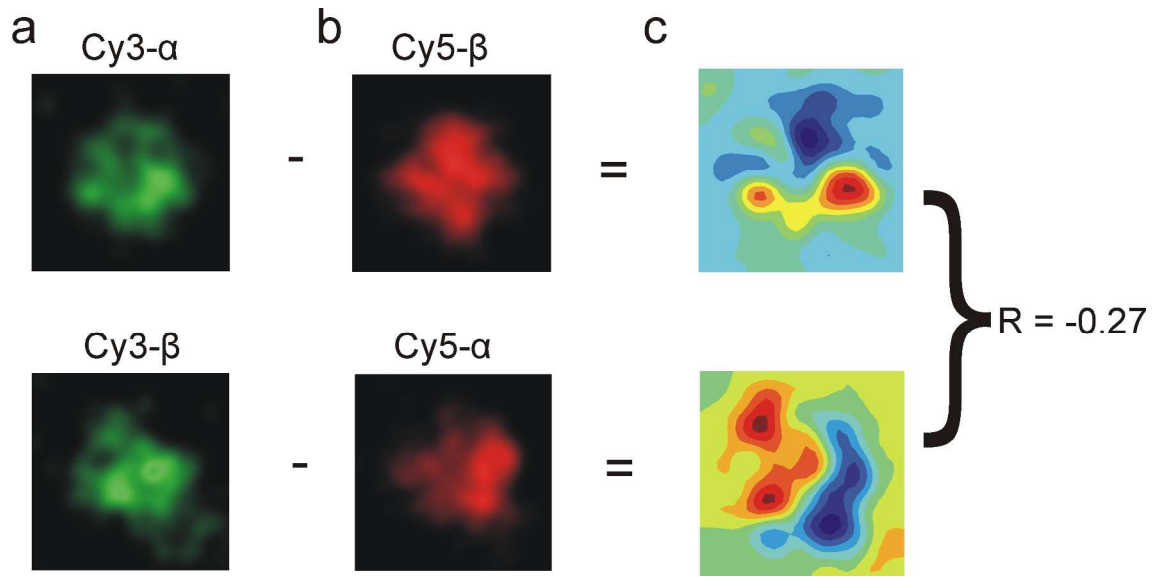

PAINT reconstructions from the same origami using two sets of probes, (**α-Cy3** + **β-Cy5**) and (**β-Cy3** + **α-Cy5**), are used to calculate intensity difference maps to investigate the dependence of binding distributions on probe sequence. For each probe set, the normalized Cy5 reconstruction of a single origami (**b**) is subtracted from the normalized Cy3 reconstruction (**a**), yielding an intensity difference map (**c**). The correlation coefficient between the difference maps from the two probe sets is then calculated. A negative correlation coefficient is expected if there is sequence-dependent heterogeneity of binding that persists over the approximately 1 h between imaging experiments.

Figure S11 – Determination of Assembly Yield by AFM

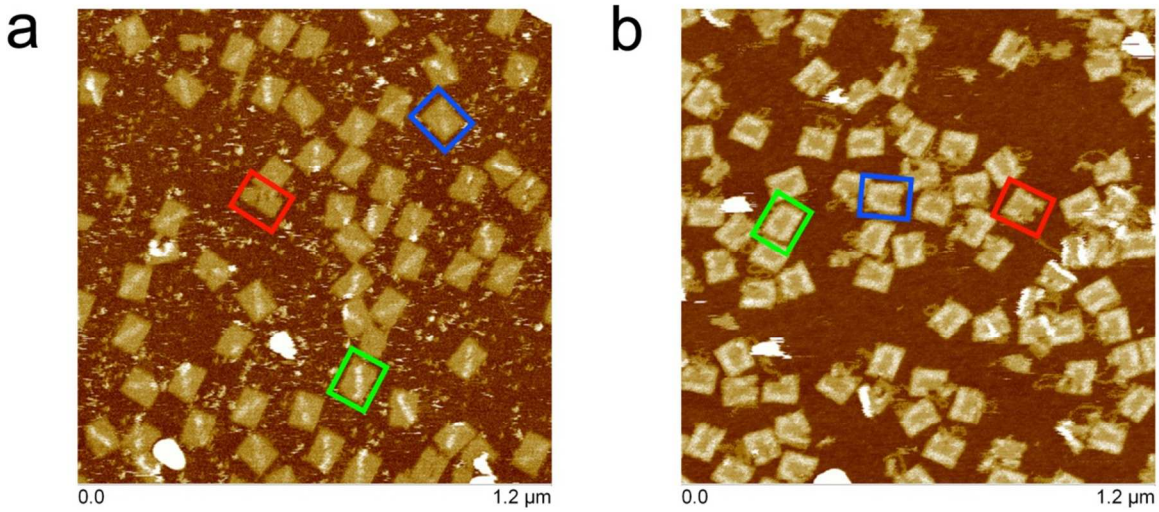

a, b, Representative AFM images of R **(a)** and L **(b)** origami, respectively, used for classification of assembly yield. In the images, the green, blue, and red rectangles depict origami tiles with different statuses. The green rectangles denote origami tiles that are clearly well formed with evidence of a fairly complete **S** pattern. The blue rectangles indicate origami tiles that are well formed with defective or missing **S** pattern. The red rectangles represent origami tiles that are broken or deformed. Each DNA origami structure in the AFM images shown here (and additional images not shown) was assigned to one of the three previously described categories. See Table S3 for the results of this analysis.

Figure S12: Denaturing Polyacrylamide Gel Characterization of Substrate

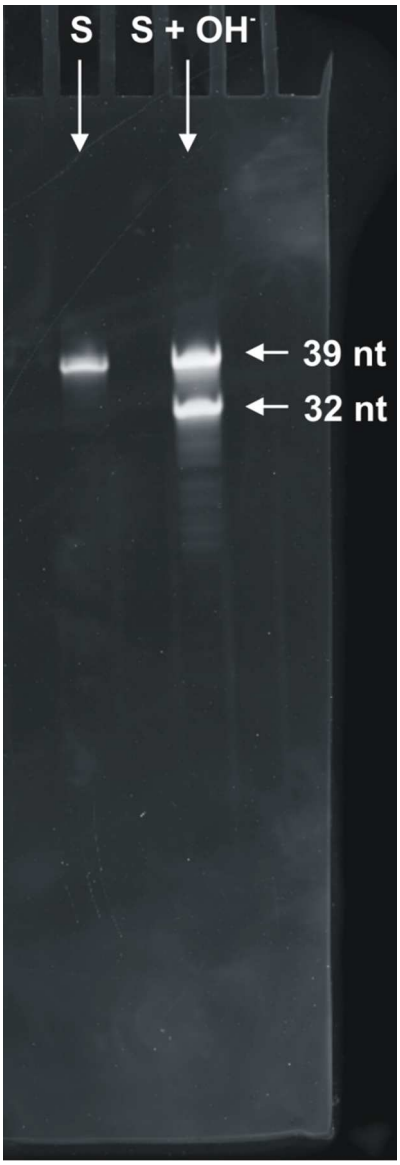

Comparison of substrate (**S**, lane 1) to an alkaline hydrolysis ladder of the substrate (**S** + OH^-, lane 2) in a 20% polyacrylamide gel containing 8 M urea. The bands are visualized using SYBR Gold. The upper band is full-length **S** (39 nt), while the lower band is the longer of two cleavage products (32 nt). No cleavage product band is detected in lane 1. The shorter product (7 nt) is not visibly stained.

Figure S13: Origami for measuring dependence of PAINT probe binding kinetics on substrate density

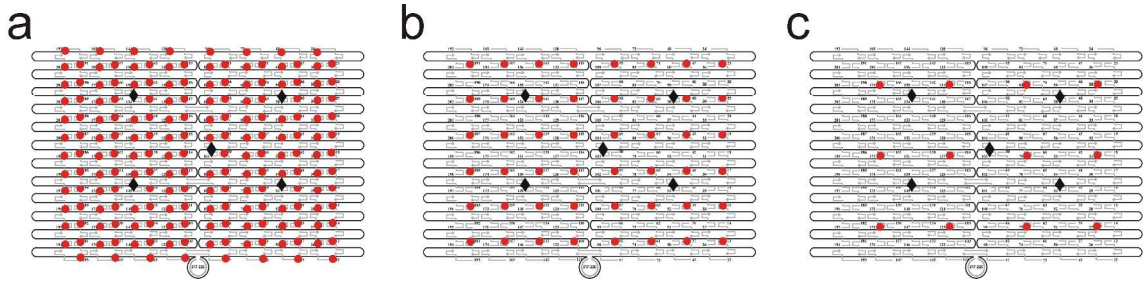

Origami with different distances between nearest-neighbor **S** strands: (a) **D5** (5 nm), (b) **D10** (10 nm), and (c) **D20** (20 nm). Origami tiles bear 187, 48, or 12 copies of **S** (red dots) and five biotins (black diamonds) on opposite faces of the tile.

Figure S14: Two competing, plausible models for the effects of local substrate concentration on probe-substrate binding

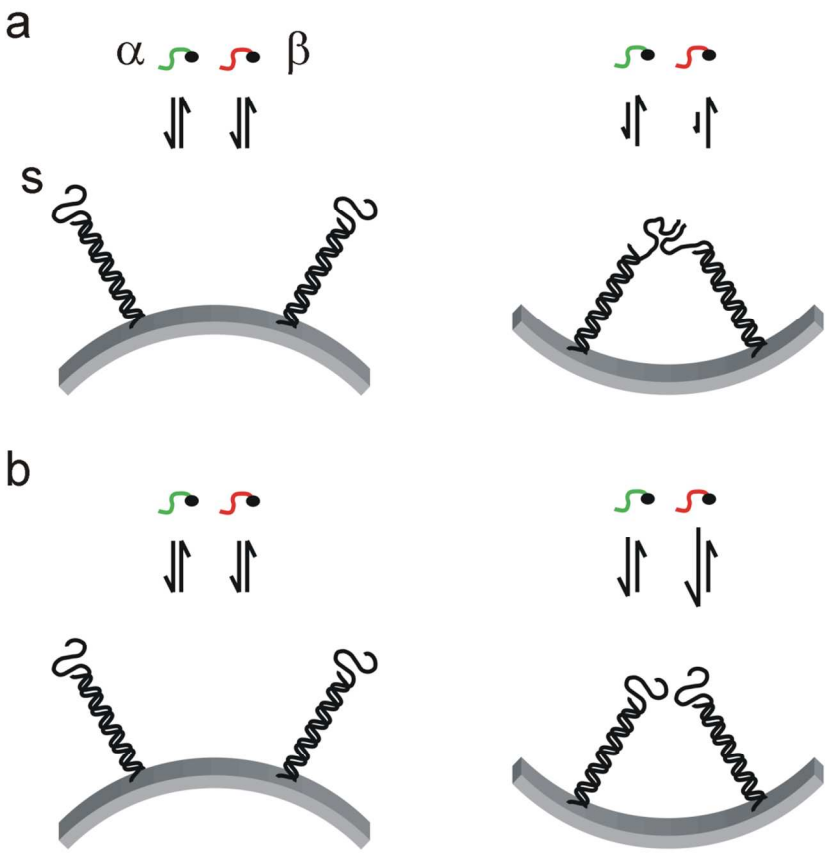

(a) Inhibitory model and (b) cooperative model. Relative lengths of on-off rate arrows illustrate reduced versus enhanced on-rates. In the inhibitory model, we hypothesize that weak, non-Watson-Crick interactions between nearest-neighbor **S** strands reduce the effective on-rate of PAINT probe binding to **S**, with this effect enhanced when the tile is bent such that strands splay inwards (right) versus outwards (left). In contrast, in the cooperative model we hypothesize that proximity of nearest-neighbor substrates increases the effective on-rate by, for instance, increasing the probability of a productive encounter, with this effect reduced when the tile is bent such that target sites splay outwards (left) versus inwards (right). In both models, the proximity of substrates is expected to influence the binding of **β** to a greater extent than **α** because the ssDNA sequence to which **β** binds is located distal to alpha on **S**.

Figure S15: Predicted three-dimensional solution shapes of R origami

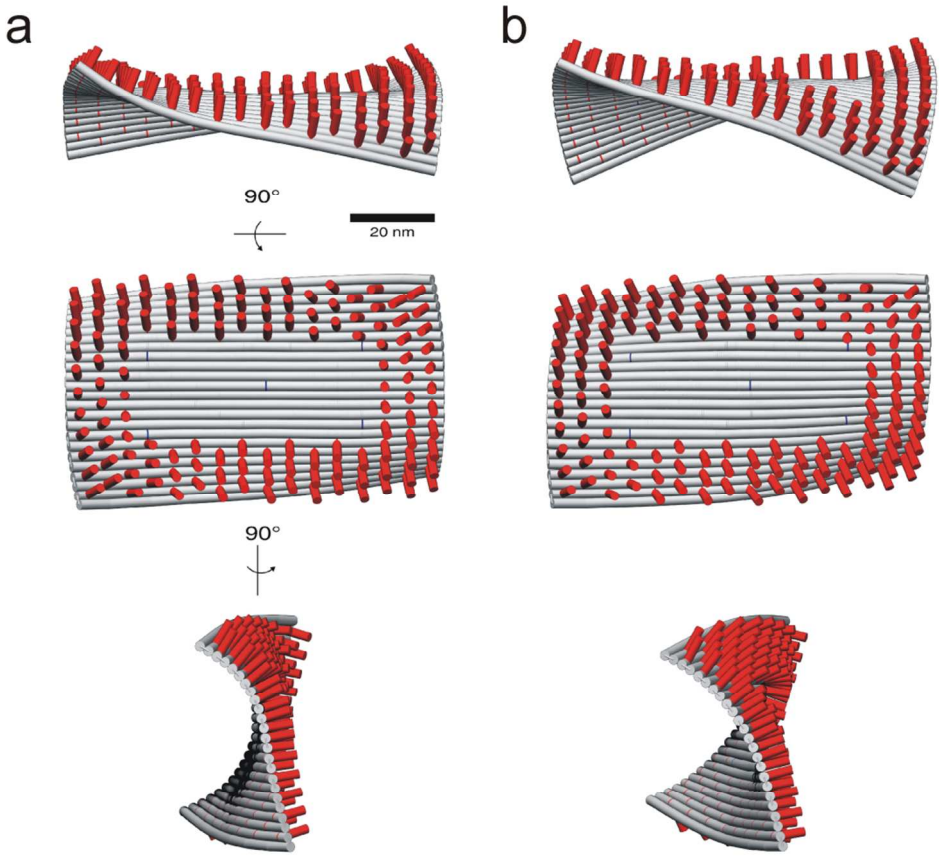

Predicted three-dimensional solution shape of R origami in three orthogonal views, when (a) the pegboard is fixed at all five biotin anchor sites (blue bands) or (b) the pegboard is constrained only in the middle. Red cylinders represent 20-base-pair double-stranded DNA segments at substrate locations that are assumed to be normal to the surface.

Figure S16: Effective relative substrate concentration on R origami

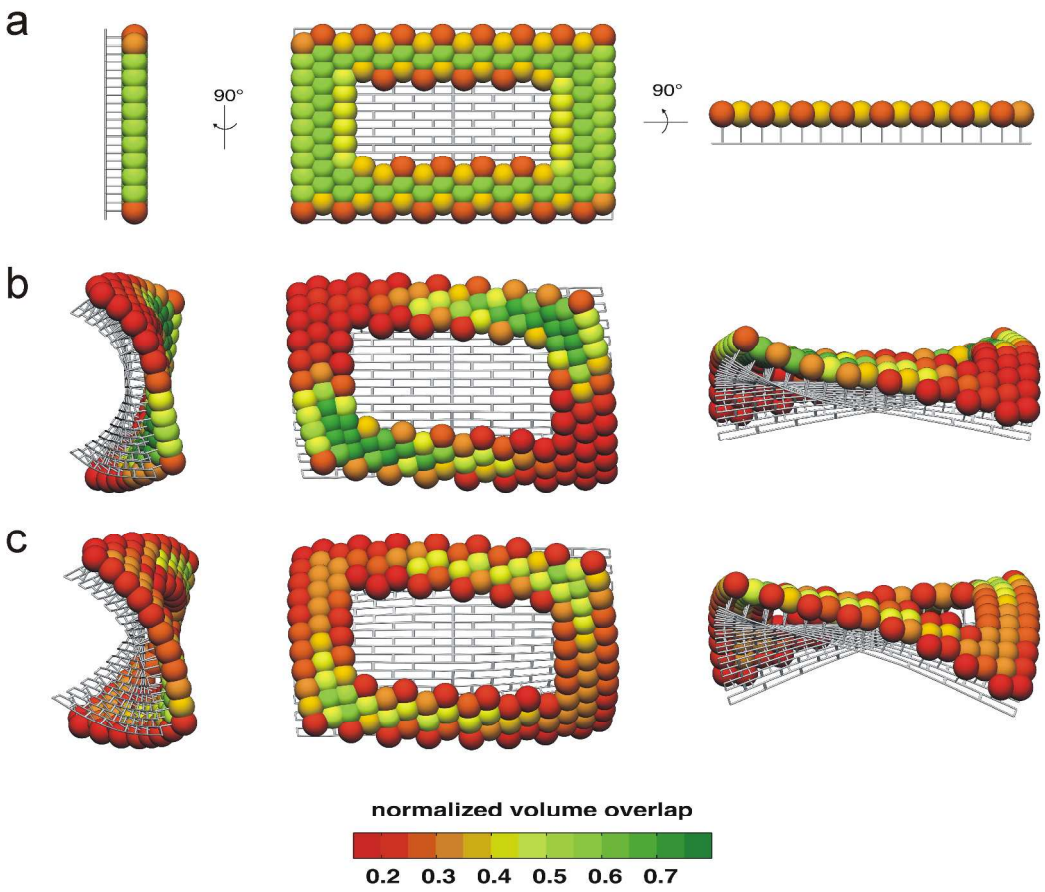

The effect of three-dimensional solution shape on effective local substrate concentration is characterized by calculating the effective volume overlap between adjacent spheres with a radius of 3.6 nm centered at the tip of 20-base-pair DNA duplexes. (a) Homogeneous pattern of the volume overlap when a flat conformation of the pegboard is assumed and (b-c) heterogeneous volume overlap patterns of curved pegboards whose three-dimensional solution shapes were computed using CanDo[9,10] (b) with and (c) without constraints at the biotin anchor sites.

Figure S17: Side-by-side comparison of predicted effective substrate concentration and two-color PAINT images

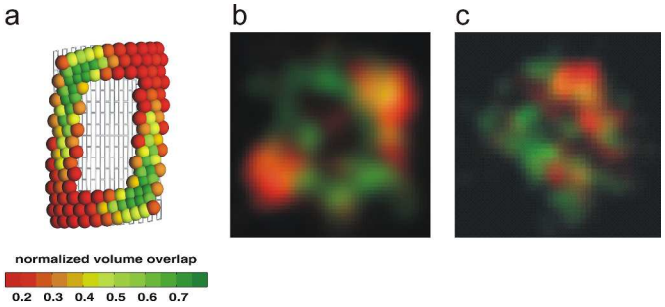

(a) Predicted pattern of effective local concentration for **R** pattern of substrates with constrained biotin positions (from Figure S16, panel (b)). (b), (c) Two **R** origami with especially heterogeneous patterns of **β-Cy5** binding (red; **α-Cy5** binding distribution in green).

Table S1: Staple Sequences

1	TTTTCGATGGCCCACTACGTAAACCGTC
2	TATCAGGGTTTTCGGTTTGCGTATTGGGAACGCGCG
3	GGGAGAGGTTTTTGTAAAACGACGGCCATTCCCAGT
4	CACGACGTTTTTGTAATGGGATAGGTCAAAACGGCG
5	GATTGACCTTTTGATGAACGGTAATCGTAGCAAACA
6	AGAGAATCTTTTGGTTGTACCAAAAACAAGCATAAA
7	GCTAAATCTTTTCTGTAGCTCAACATGTATTGCTGA
8	ATATAATGTTTTCATTGAATCCCCCTCAAATCGTCA
9	TAAATATTTTTTGGAAGAAAAATCTACGACCAGTCA
10	GGACGTTGTTTTTCATAAGGGAACCGAAAGGCGCAG
11	ACGGTCAATTTTGACAGCATCGGAACGAACCCTCAG
12	CAGCGAAAATTTTACTTTCAACAGTTTCTGGGATTTTGCTAAACTTTT
13	TGGTTTTTAACGTCAAAGGGCGAAGAACCATC
14	CTTGCATGCATTAATGAATCGGCCCGCCAGGG
15	TAGATGGGGGGTAACGCCAGGGTTGTGCCAAG
16	CATGTCAAGATTCTCCGTGGGAACCGTTGGTG
17	CTGTAATATTGCCTGAGAGTCTGGAAAACTAG
18	TGCAACTAAGCAATAAAGCCTCAGTTATGACC
19	AAACAGTTGATGGCTTAGAGCTTATTTAAATA
20	ACGAACTAGCGTCCAATACTGCGGAATGCTTT
21	CTTTGAAAAGAACTGGTCCTCTTTTGAGGAACAAGTTTTCTTGT CTCATTATTTAATAAA
22	ACGGCTACTTACTTAGTCCTCTTTTGAGGAACAAGTTTTCTTGT CCGGAACGCTGACCAA
23	GAGAATAGCTTTTGCGGGATCGTCGGGTAGCA
24	ACGTTAGTAAATGAATTTTCTGTAAGCGGAGT
25	ACCCAAATCAAGTTTTTTGGGGTCAAAGAACG
26	TGGACTCCCTTTTCACCAGTGAGACCTGTCGT
27	GCCAGCTGCCTGCAGGTCGACTCTGCAAGGCG
28	ATTAAGTTCGCATCGTAACCGTGCGAGTAACA
29	ACCCGTCGTCATATGTACCCCGGTAAAGGCTA
30	TCAGGTCACTTTTGCGGGAGAAGCAGAATTAG
31	CAAAATTAAAGTACGGTGTCTGGAAGAGGTCA
32	TTTTTGCGCAGAAAACGAGAATGAATGTTTAG
33	ACTGGATAACGGAACAACATTATTACCTTATG
34	CGATTTTAGAGGACAGTCCTCTTTTGAGGAACAAGTTTTCTTGT ATGAACGGCGCGACCT
35	GCTCCATGAGAGGCTTTCCTCTTTTGAGGAACAAGTTTTCTTGT TGAGGACTAGGGAGTT
36	AAAGGCCGAAAGGAACAACTAAAGCTTTCCAG
37	AGCTGATTACAAGAGTCCACTATTGAGGTGCC
38	CCCGGGTACTTTCCAGTCGGGAAACGGGCAAC
39	GTTTGAGGGAAAGGGGGATGTGCTAGAGGATC
40	AGAAAAGCAACATTAAATGTGAGCATCTGCCA

41	CAACGCAATTTTTGAGAGATCTACTGATAATC
42	TCCATATACATACAGGCAAGGCAACTTTATTT
43	CAAAAATCATTGCTCCTTTTGATAAGTTTCAT
44	AAAGATTCAGGGGGTAATAGTAAACCATAAAT
45	CCAGGCGCTTAATCATTCCTCTTTTGAGGAACAAGTTTTCTTGT TGTGAATTACAGGTAG
46	TTTCATGAAAATTGTGTCCTCTTTTGAGGAACAAGTTTTCTTGT TCGAAATCTGTACAGA
47	AATAATAAGGTCGCTGAGGCTTGCAAAGACTT
48	CGTAACGATCTAAAGTTTTGTCGTGAATTGCG
49	GTAAAGCACTAAATCGGAACCCTAGTTGTTCC
50	AGTTTGGAGCCCTTCACCGCCTGGTTGCGCTC
51	ACTGCCCGCCGAGCTCGAATTCGTTATTACGC
52	CAGCTGGCGGACGACGACAGTATCGTAGCCAG
53	CTTTCATCCCCAAAAACAGGAAGACCGGAGAG
54	GGTAGCTAGGATAAAAATTTTTAGTTAACATC
55	CAATAAATACAGTTGATTCCCAATTTAGAGAG
56	TACCTTTAAGGTCTTTACCCTGACAAAGAAGT
57	TTTGCCAGATCAGTTGAGATTTAGTGGTTTAA
58	TTTCAACTATAGGCTGGCTGACCTTGTATCAT
59	CGCCTGATGGAAGTTTCCATTAAACATAACCG
60	ATATATTCTTTTTTCACGTTGAAAATAGTTAG
61	GAGTTGCACGAGATAGGGTTGAGTAAGGGAGC
62	TCATAGCTACTCACATTAATTGCGCCCTGAGA
63	GAAGATCGGTGCGGGCCTCTTCGCAATCATGG
64	GCAAATATCGCGTCTGGCCTTCCTGGCCTCAG
65	TATATTTTAGCTGATAAATTAATGTTGTATAA
66	CGAGTAGAACTAATAGTAGTAGCAAACCCTCA
67	TCAGAAGCCTCCAACAGGTCAGGATCTGCGAA
68	CATTCAACGCGAGAGGCTTTTGCATATTATAG
69	AGTAATCTTAAATTGGGCTTGAGAGAATACCA
70	ATACGTAAAAGTACAACGGAGATTTCATCAAG
71	AAAAAAGGACAACCATCGCCCACGCGGGTAAA
72	TGTAGCATTCCACAGACAGCCCTCATCTCCAA
73	CCCCGATTTAGAGCTTGACGGGGAAATCAAAA
74	GAATAGCCGCAAGCGGTCCACGCTCCTAATGA
75	GTGAGCTAGTTTCCTGTGTGAAATTTGGGAAG
76	GGCGATCGCACTCCAGCCAGCTTTGCCATCAA
77	AAATAATTTTAAATTGTAAACGTTGATATTCA
78	ACCGTTCTAAATGCAATGCCTGAGAGGTGGCA
79	TCAATTCTTTTAGTTTGACCATTACCAGACCG
80	GAAGCAAAAAAGCGGATTGCATCAGATAAAAA
81	CCAAAATATAATGCAGATACATAAACACCAGA

82	ACGAGTAGTGACAAGAACCGGATATACCAAGC
83	GCGAAACATGCCACTACGAAGGCATGCGCCGA
84	CAATGACACTCCAAAAGGAGCCTTACAACGCC
85	CCAGCAGGGGCAAAATCCCTTATAAAGCCGGC
86	GCTCACAATGTAAAGCCTGGGGTGGGTTTGCC
87	GCTTCTGGTCAGGCTGCGCAACTGTGTTATCC
88	GTTAAAATTTTAACCAATAGGAACCCGGCACC
89	AGGTAAAGAAATCACCATCAATATAATATTTT
90	TCGCAAATGGGGCGCGAGCTGAAATAATGTGT
91	AAGAGGAACGAGCTTCAAAGCGAAGATACATT
92	GGAATTACTCGTTTACCAGACGACAAAAGATT
93	CCAAATCACTTGCCCTGACGAGAACGCCAAAA
94	AAACGAAATGACCCCCAGCGATTATTCATTAC
95	TCGGTTTAGCTTGATACCGATAGTCCAACCTA
96	TGAGTTTCGTCACCAGTACAAACTTAATTGTA
97	GAACGTGGCGAGAAAGGAAGGGAACAAACTAT
98	CCGAAATCCGAAAATCCTGTTTGAAGCCGGAA
99	GCATAAAGTTCCACACAACATACGAAGCGCCA
100	TTCGCCATTGCCGGAAACCAGGCATTAAATCA
101	GCTCATTTTCGCATTAAATTTTTGAGCTTAGA
102	AGACAGTCATTCAAAAGGGTGAGAAGCTATAT
103	TTTCATTTGGTCAATAACCTGTTTATATCGCG
104	TTTTAATTGCCCGAAAGACTTCAAAACACTAT
105	CATAACCCGAGGCATAGTAAGAGCTTTTTAAG
106	GAATAAGGACGTAACAAAGCTGCTCTAAAACA
107	CTCATCTTGAGGCAAAAGAATACAGTGAATTT
108	CTTAAACATCAGCTTGCTTTCGAGCGTAACAC
109	ACGAACCAAAACATCGCCATTAAATGGTGGTT
110	CGACAACTAAGTATTAGACTTTACAATACCGA
111	CTTTTACACAGATGAATATACAGTAAACAATT
112	TTAAGACGTTGAAAACATAGCGATAACAGTAC
113	GCGTTATAGAAAAAGCCTGTTTAGAAGGCCGG
114	ATCGGCTGCGAGCATGTAGAAACCTATCATAT
115	CCTAATTTACGCTAACGAGCGTCTAATCAATA
116	AAAAGTAATATCTTACCGAAGCCCTTCCAGAG
117	TTATTCATAGGGAAGGTAAATATTCATTCAGT
118	GAGCCGCCCCACCACCGGAACCGCGACGGAAA
119	AATGCCCCGTAACAGTGCCCGTATCTCCCTCA
120	CAAGCCCAATAGGAACCCATGTACAAACAGTT
121	CGGCCTTGCTGGTAATATCCAGAACGAACTGA
122	TAGCCCTACCAGCAGAAGATAAAAACATTTGA

123	GGATTTAGCGTATTAAATCCTTTGTTTTCAGG
124	TTTAACGTTCGGGAGAAACAATAATTTTCCCT
125	TAGAATCCCTGAGAAGAGTCAATAGGAATCAT
126	AATTACTACAAATTCTTACCAGTAATCCCATC
127	CTAATTTATCTTTCCTTATCATTCATCCTGAA
128	TCTTACCAGCCAGTTACAAAATAAATGAAATA
129	GCAATAGCGCAGATAGCCGAACAATTCAACCG
130	ATTGAGGGTAAAGGTGAATTATCAATCACCGG
131	AACCAGAGACCCTCAGAACCGCCAGGGGTCAG
132	TGCCTTGACTGCCTATTTCGGAACAGGGATAG
133	AGGCGGTCATTAGTCTTTAATGCGCAATATTA
134	TTATTAATGCCGTCAATAGATAATCAGAGGTG
135	CCTGATTGAAAGAAATTGCGTAGACCCGAACG
136	ATCAAAATCGTCGCTATTAATTAACGGATTCG
137	ACGCTCAAAATAAGAATAAACACCGTGAATTT
138	GGTATTAAGAACAAGAAAAATAATTAAAGCCA
139	ATTATTTAACCCAGCTACAATTTTCAAGAACG
140	GAAGGAAAATAAGAGCAAGAAACAACAGCCAT
141	GACTTGAGAGACAAAAGGGCGACAAGTTACCA
142	GCCACCACTCTTTTCATAATCAAACCGTCACC
143	CTGAAACAGGTAATAAGTTTTAACCCCTCAGA
144	CTCAGAGCCACCACCCTCATTTTCCTATTATT
145	CCGCCAGCCATTGCAACAGGAAAAATATTTTT
146	GAATGGCTAGTATTAACACCGCCTCAACTAAT
147	AGATTAGATTTAAAAGTTTGAGTACACGTAAA
148	ACAGAAATCTTTGAATACCAAGTTCCTTGCTT
149	CTGTAAATCATAGGTCTGAGAGACGATAAATA
150	AGGCGTTACAGTAGGGCTTAATTGACAATAGA
151	TAAGTCCTACCAAGTACCGCACTCTTAGTTGC
152	TATTTTGCTCCCAATCCAAATAAGTGAGTTAA
153	GCCCAATACCGAGGAAACGCAATAGGTTTACC
154	AGCGCCAACCATTTGGGAATTAGATTATTAGC
155	GTTTGCCACCTCAGAGCCGCCACCGATACAGG
156	AGTGTACTTGAAAGTATTAAGAGGCCGCCACC
157	GCCACGCTATACGTGGCACAGACAACGCTCAT
158	ATTTTGCGTCTTTAGGAGCACTAAGCAACAGT
159	GCGCAGAGATATCAAAATTATTTGACATTATC
160	TAACCTCCATATGTGAGTGAATAAACAAAATC
161	CATATTTAGAAATACCGACCGTGTTACCTTTT
162	CAAGCAAGACGCGCCTGTTTATCAAGAATCGC
163	TTTTGTTTAAGCCTTAAATCAAGAATCGAGAA

164	ATACCCAAGATAACCCACAAGAATAAACGATT
165	AATCACCAAATAGAAAATTCATATATAACGGA
166	CACCAGAGTTCGGTCATAGCCCCCGCCAGCAA
167	CCTCAAGAATACATGGCTTTTGATAGAACCAC
168	CCCTCAGAACCGCCACCCTCAGAACTGAGACT
169	GGAAATACCTACATTTTGACGCTCACCTGAAA
170	GCGTAAGAGAGAGCCAGCAGCAAAAAGGTTAT
171	CTAAAATAGAACAAAGAAACCACCAGGGTTAG
172	AACCTACCGCGAATTATTCATTTCCAGTACAT
173	AAATCAATGGCTTAGGTTGGGTTACTAAATTT
174	AATGGTTTACAACGCCAACATGTAGTTCAGCT
175	AATGCAGACCGTTTTTATTTTCATCTTGCGGG
176	AGGTTTTGAACGTCAAAAATGAAAGCGCTAAT
177	ATCAGAGAAAGAACTGGCATGATTTTATTTTG
178	TCACAATCGTAGCACCATTACCATCGTTTTCA
179	TCGGCATTCCGCCGCCAGCATTGACGTTCCAG
180	TAAGCGTCGAAGGATTAGGATTAGTACCGCCA
181	CTAAAGCAAGATAGAACCCTTCTGAATCGTCT
182	CGGAATTATTGAAAGGAATTGAGGTGAAAAAT
183	GAGCAAAAACTTCTGAATAATGGAAGAAGGAG
184	TATGTAAACCTTTTTTAATGGAAAAATTACCT
185	AGAGGCATAATTTCATCTTCTGACTATAACTA
186	TCATTACCCGACAATAAACAACATATTTAGGC
187	CTTTACAGTTAGCGAACCTCCCGACGTAGGAA
188	TTATTACGGTCAGAGGGTAATTGAATAGCAGC
189	CCGGAAACACACCACGGAATAAGTAAGACTCC
190	TGAGGCAGGCGTCAGACTGTAGCGTAGCAAGG
191	TGCTCAGTCAGTCTCTGAATTTACCAGGAGGT
192	TATCACCGTACTCAGGAGGTTTAGCGGGGTTT
193	GAAATGGATTATTTACATTGGCAGACATTCTG
194	GCCAACAGTCACCTTGCTGAACCTGTTGGCAA
195	ATCAACAGTCATCATATTCCTGATTGATTGTT
196	TGGATTATGAAGATGATGAAACAAAATTTCAT
197	TTGAATTATGCTGATGCAAATCCACAAATATA
198	TTTTAGTTTTTCGAGCCAGTAATAAATTCTGT
199	CCAGACGAGCGCCCAATAGCAAGCAAGAACGC
200	GAGGCGTTAGAGAATAACATAAAAGAACACCC
201	TGAACAAACAGTATGTTAGCAAACTAAAAGAA
202	ACGCAAAGGTCACCAATGAAACCAATCAAGTT
203	TGCCTTTAGTCAGACGATTGGCCTGCCAGAAT
204	GGAAAGCGACCAGGCGGATAAGTGAATAGGTG

205	AAACCCTCTTTTACCAGTAATAAAAGGGATTCACCAGTCACACGTTTT
206	GATGGCAATTTTAATCAATATCTGGTCACAAATATC
207	AAAACAAATTTTTTCATCAATATAATCCTATCAGAT
208	ACAAAGAATTTTATTAATTACATTTAACACATCAAG
209	TAAAGTACTTTTCGCGAGAAAACTTTTTATCGCAAG
210	TATAGAAGTTTTCGACAAAAGGTAAAGTAGAGAATA
211	GCGCATTATTTTGCTTATCCGGTATTCTAAATCAGA
212	TACATACATTTTGACGGGAGAATTAACTACAGGGAA
213	AGCACCGTTTTTTAAAGGTGGCAACATAGTAGAAAA
214	ACAAACAATTTTAATCAGTAGCGACAGATCGATAGC
215	AGGGTTGATTTTATAAATCCTCATTAAATGATATTC
216	TTTTTATAAGTATAGCCCGGCCGTCGAG
217	AACATCACTTGCCTGAGTAGAAGAACT
218	TGTAGCAATACTTCTTTGATTAGTAAT
219	AGTCTGTCCATCACGCAAATTAACCGT
220	ATAATCAGTGAGGCCACCGAGTAAAAG
221	ACGCCAGAATCCTGAGAAGTGTTTTT
222	TTAAAGGGATTTTAGACAGGAACGGT
223	AGAGCGGGAGCTAAACAGGAGGCCGA
224	TATAACGTGCTTTCCTCGTTAGAATC
225	GTACTATGGTTGCTTTGACGAGCACG
226	GCGCTTAATGCGCCGCTACAGGGCGC

All sequences in Table S1 are listed from 5′ to 3′ and correspond to unmodified staples. Biotin modifications were performed as follows: for **R**, **D5**, **D10**, and **D20** tiles, staples 53, 57, 103, 160, and 164 were divided into two 18 nucleotide long staples and one of the resulting fragments was modified with a biotin molecule at the 5′ end. For **L** tiles, staples 3, 11, 206, and 214 were similarly divided and modified.

For **R** tiles, the following staples were modified with the substrate binding probe sequence at the 5′ end: 13, 14, 15, 16, 17, 18, 19, 20, 21, 22, 23, 26, 27, 28, 29, 30, 31, 32, 33, 34, 35, 36, 37, 38, 39, 40, 41, 42, 43, 44, 45, 46, 47, 50, 51, 52, 58, 59, 60, 61, 62, 63, 69, 70, 71, 74, 75, 76, 82, 83, 84, 85, 86, 87, 93, 94, 95, 98, 99, 100, 106, 107, 108, 109, 110, 111, 117, 118, 119, 122, 123, 124, 130, 131, 132, 133, 134, 135, 141, 142, 143, 146, 147, 148, 154, 155, 156, 157, 158, 159, 165, 166, 167, 170, 171, 172, 173, 174, 175, 176, 177, 178, 179, 180, 181, 182, 183, 184, 185, 186, 187, 188, 189, 190, 191, 194, 195, 196, 197, 198, 199, 200, 201, 202, 203, 204

For **L** tiles, the following staples were modified with the substrate binding probe sequence at the 5′ end: 13, 14, 25, 26, 27, 28, 37, 38, 39, 51, 52, 53, 62, 63, 64, 76, 77,

78, 87, 88, 89, 101, 102, 103, 112, 113, 114, 126, 127, 128, 137, 138, 139, 151, 152, 153, 162, 163, 164, 176, 177, 178

For **D5** tiles, the following staples were modified with the substrate binding probe sequence at the 5′ end: 13-52, 54-57,59-102,104-148,150-211

For **D10** tiles, the following staples were modified with the substrate binding probe sequence at the 5′ end: 13, 15, 17, 19, 21, 23, 37, 39, 41, 43, 45, 61, 63, 65, 67, 69, 71, 85, 87, 89, 91, 93, 95, 109, 111, 113, 115, 117, 119, 133, 135, 137, 139, 141, 143, 157, 159, 161, 163, 165, 167, 181, 183, 185, 187, 189, 191

For **D20** tiles, the following staples were modified with the substrate binding probe sequence at the 5′ end: 27, 31, 35, 75, 79, 83, 123, 127, 131, 171, 175, 179

Table S2: Kinetics of Probe Strand Binding to R Origami

Probe Strand	$k_{on,R}$ **(x 10^7 M^{-1} s^{-1})**	k_{off} **(s^{-1})**
α-Cy3	1.98 ± 0.04	0.34 ± 0.01
β-Cy5	2.03 ± 0.03	0.22 ± 0.03

Error bars are 1 s.e.m from duplicate measurements. $k_{on,R}$ represents the apparent second-order rate constant of probe binding to an **R** origami tile with up to 126 copies of **S**. Kinetic characterization was conducted under ~10% maximal illumination to limit photobleaching, and results were insensitive to a two-fold change in excitation intensity (data not shown).

Table S3: Yield of R and L Tiles and Patterns Determined by AFM

Status	**R (N = 592)**	**L (N = 564)**
Well-formed tile with clear evidence of fairly complete **S** pattern	30.1% (178/592)	65.2% (368/564)
Well-formed tile with defective or missing **S** pattern	21.8% (129/592)	7.3% (41/564)
Broken or deformed tile	48.1% (285/592)	27.5% (155/564)

Supporting References

(1) Lund, K.; Manzo, A. J.; Dabby, N.; Michelotti, N.; Johnson-Buck, A.; Nangreave, J.; Taylor, S.; Pei, R.; Stojanovic, M. N.; Walter, N. G.; Winfree, E.; Yan, H. *Nature 465*, 206–210.
(2) Michelotti, N.; de Silva, C.; Johnson-Buck, A. E.; Manzo, A. J.; Walter, N. G. *Methods Enzymol.* **2010**, *475*, 121–148.
(3) Aitken, C. E.; Marshall, R. A.; Puglisi, J. D. *Biophys. J.* **2008**, *94*, 1826–1835.
(4) Bronson, J. E.; Fei, J.; Hofman, J. M.; Gonzalez Jr., R. L.; Wiggins, C. H. *Biophys. J.* **2009**, *97*, 3196–3205.
(5) Guizar-Sicairos, M.; Thurman, S. T.; Fienup, J. R. *Opt. Lett.* **2008**, *33*, 156–158.
(6) Thompson, R. E.; Larson, D. R.; Webb, W. W. *Biophys. J.* **2002**, *82*, 2775–2783.
(7) Churchman, L. S.; Ökten, Z.; Rock, R. S.; Dawson, J. F.; Spudich, J. A. *Proc. Nat. Acad. Sci. U.S.A.* **2005**, *102*, 1419–1423.
(8) Potthoff, R. F.; Whittinghill, M. *Biometrika* **1966**, *53*, 183–190.
(9) Kim, D.-N.; Kilchherr, F.; Dietz, H.; Bathe, M. *Nucleic Acids Res.* **2012**, *40*, 2862–2868.
(10) Castro, C. E.; Kilchherr, F.; Kim, D.-N.; Shiao, E. L.; Wauer, T.; Wortmann, P.; Bathe, M.; Dietz, H. *Nat. Methods* **2011**, *8*, 221–229.
(11) Smith, S. B.; Cui, Y.; Bustamante, C. *Science* **1996**, *271*, 795–799.